ISSN 1392-1207. MECHANIKA. Vol. 30, No. 1, 2024: 46–56

Kinematics and Trajectory Planning of 3-PSS/7R Spatial Hybrid Redundantly Driven Mechanism

Qisheng ZHANG*, Ruiqin LI， Jingjing LIANG***, Yao WEI******
**School of Mechanical Engineering, North University of China, Taiyuan 030051, China,*
E-mail: zhangqisheng_qs@nuc.edu.cn
***School of Mechanical Engineering, North University of China, Taiyuan 030051, China, E-mail: liruiqin@nuc.edu.cn (Corresponding author)*
****School of Mechanical Engineering, North University of China, Taiyuan 030051, China, E-mail: 944719179@qq.com*
*****North of England Robotic Innovation Centre, University of Salford, Manchester M6 6AP, UK,*
E-mail: w.yao@salford.ac.uk
https://doi.org/10.5755/j02.mech.30862

1. Introduction

"Hybrid machine" was first proposed by Tokuz and Jones from Liverpool University of Technology in the 1990s [1]. Hybrid driven mechanism (HDM for short), also known as hybrid input mechanism, is a type of controllable mechanism. HDM is different from full servo drive mechanism, which uses constant velocity (CV for short) motors and servo motors to drive a multi-DOF mechanical system to output flexible and controllable trajectory. HDM is between controllable mechanism and uncontrollable mechanism, and has certain flexibility. At present, HDM has become an important branch in the field of modern mechanisms, which has the advantages of large carrying capacity, strong driving force and low cost.

At present, the research on hybrid driven two-DOF planar multi-bar mechanism is the most in-depth, such as hybrid driven planar five-bar mechanism, seven-bar mechanism and nine-bar mechanism. The planar five-bar mechanism has the least number of links and the most research in the two-DOF mechanisms. The theoretical research results include configuration design, mobility, trajectory planning, power matching, kinematics, dynamics, etc. [2-12]. HDM has been applied in many fields, especially press machine [6-8] and walking robot [9] are the most widely used.

The above research on HDM is mostly based on the research of planar linkage mechanism. In the process of HDM expanding from planar configuration to spatial configuration, a kind of hybrid driven parallel mechanism with flexible cable mechanism as limbs appears. Zi Bin [13-15] et al. designed a kind of hybrid-driven flexible cable parallel mechanism, which is composed of several symmetrically distributed limbs, static platform and moving platform. The composition of each limb is the same, which is composed of a hybrid-driven planar five-bar mechanism and a cable in series. The five-bar mechanism is fixed on the frame and symmetrically distributed on static platform. The lengths of the cables are jointly controlled by CV motor and servo motor, so that the moving platform can output a flexible and controllable trajectory. The remarkable characteristics of the mechanism are large workspace, large power and large load. The disadvantage is that numbers of motors is twice the degrees of freedom, which brings difficulties to the control of the system. The dynamics, workspace and singular space, system control, trajectory planning, performance optimization, stiffness, system reliability and error of such mechanisms have been studied [13-18].

As a scheme of hybrid-driven spatial mechanism [19, 20], hybrid redundantly driven mechanism (HRDM for short) has the characteristics of HDM and RDM. n-DOF HRDM has $n + 1$ limbs, of which n driving limbs with 6-DOF are symmetrically distributed between the moving platform and the static platform, which does not restrict the DOFs of the mechanism; An intermediate limb is driven by CV motor and servo motor simultaneously, which restricts the DOFs of the mechanism. Because of the uncontrollable characteristics of CV motor, the flexibility of the mechanism decreases and the output DOFs decreases, which is mainly used in the field of lower-mobility. The output of the moving platform of lower-mobility HRDM is less than six DOFs. Compared with 6-DOF HRDM, lower-mobility HRDM only needs fewer driving motors, whose structure is simple and the control is convenient. It can well satisfy the characteristic requirements of partial flexibility for the motion output of the mechanism. It has broad application prospects in the fields of aerospace, disaster rescue and medical rehabilitation, etc.

In this paper, a geometrical model of 3-DOF 3-PSS/7R spatial HRDM is proposed. The inverse kinematics characteristics of the mechanism are analyzed by establishing the position equation and acceleration equation of 3-PSS/7R HRDM. The motion continuity of each kinematic pair and influence of the initial configuration on the included angle of the intermediate limb and the compensation angle of servo motor are studied. The sufficient and necessary conditions for accurately realizing the trajectory planning of the mechanism are studied. Simulation results verify that the mechanism can realize continuous trajectory and inverse kinematic solution is unique.

The paper is organized as follows: Section 2 introduces the geometrical model of 3-PSS/7R HRDM. The kinematic modeling of the mechanism is established in Section 3. In Section 4, the necessary and sufficient conditions for smooth and continuous trajectory of the HRDM are derived. In Section 5, the correctness of the kinematic model and the controllability of the mechanism are demonstrated. Finally, conclusions are drawn in Section 6.

2. Geometrical model of 3-PSS/7R HRDM

The 3D model of 3-PSS/7R HRDM studied in the

paper is shown in Fig. 1, and the kinematic diagram is shown in Fig. 2. The mechanism is composed of a moving platform, a static platform and four driving limbs. Three PSS limbs (P is prismatic pair and S is spherical pair) have the same configuration and are symmetrically distributed between the moving platform and the static platform, which does not restrict the DOFs of the HRDM. The intermediate 7R limb is composed of a planar five-bar mechanism *CDEFG* and a link *EO'* in series, and each link is connected to each other by a revolute pair.

The mechanism has three DOFs, but there are four limbs and five drives, thus the drives are redundant. The intermediate 7R limb is jointly driven by CV motor and servo motor, which is called hybrid redundantly driven limb (HRDL for short). The CV motor drives link *CD*, and the included angle between *CD* and *X*-axis is denoted as q_1. The servo motor drives link *GF*, and the included angle between link *GF* and *X*-axis is denoted as q_4. The HRDL imposes constraints on freedoms of the whole mechanism, which restricts the translation of the moving platform along Z_2-axis and the rotations around X_2-axis and Y_2-axis. Thus, the mechanism has three DOFs (two translations and one rotation, i.e. 2T1R). The link *CD* driven by CV motor and link *FG* driven by servo motor are coupled at *E* point, and through link *EO'* act on the moving platform center *O'*. The

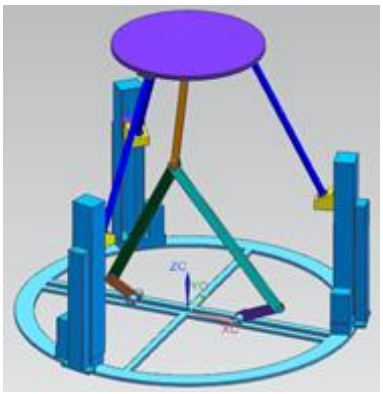

Fig. 1 3D model of 3-PSS/7R HRDM

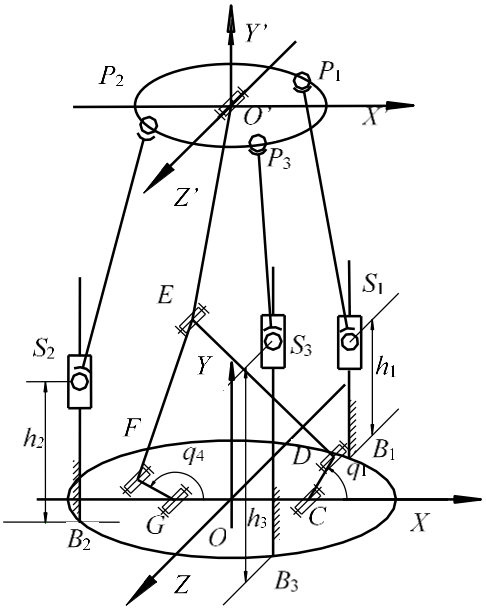

Fig. 2 The kinematic diagram of 3-PSS/7R HRDM

end orientation of limb *CDEO'* and limb *GFEO'* is the orientation of the HRDM.

Under working condition, the driving angular displacement q_1 and the initial angle q_{10} of CV motor are determined. By changing the displacement h_i (i = 1, 2, 3) of the driving links in three PSS limbs and the driving angle displacement q_4 driven by the servo motor in the HRDL, the moving platform of the HRDM can achieve three DOFs movement in the workspace.

The structure parameter of HRDM expressed as，
$|CD|=l_1$, $|DE|=l_2$, $|EF|=l_3$, $|FG|=l_4$, $|GO|=l_5$, $|OC|=l_6$, $|EO'|=l_7$.

3. Kinematic analysis of 3-PSS/7R HRDM

3.1. Mechanism position analysis of 3-PSS/7R HRDM

In Fig. 2, assume that the static coordinate system *O-XYZ* is established with the geometric center *O* of the static platform as the origin, and the moving coordinate system *O'-X'Y'Z'* is also established with the geometric center *O'* of the moving platform as the origin. The axes of the prismatic pairs of three PSS limbs intersect with the static platform at point B_i (i = 1, 2, 3), and point B_i is evenly distributed on the circumference of the static platform with the radius *R*, and the spherical hinge center P_i (i=1, 2, 3) is evenly distributed on the circumference of the moving platform with the radius *r*. $\angle P_iO'P_j=120°\ (i,j=1,2,3,i\neq j)$. When the mechanism is in the initial state, *Y*-axis and *Y'*-axis are coaxial, and *X*-axis and *Z*-axis are parallel to *X'*-axis and *Z'*-axis, respectively.

It is known that trajectory $\boldsymbol{X}=[x,y,\alpha]$ of the geometric center of the moving platform of 3-PSS/7R HRDM is continuous, thus $\dot{\boldsymbol{X}}=[\dot{x}(t),\dot{y}(t),\dot{\alpha}(t)]$ exists everywhere in the workspace. The inverse position solution is to calculate the displacement h_i (i = 1, 2, 3) of three prismatic pairs and the driving angular displacement q_4 of servo motor in the HRDL, when given the position and orientation $\boldsymbol{X}$ of the moving platform and the angular displacement q_1 of CV motor.

The inverse kinematics of the 3-PSS/7R HRDM is to solve the displacement h_i (i = 1, 2, 3) of driving slider S_i in three PSS limbs and rotation angle of the servo motor for the given position and orientation $(x,y,z,\alpha,\beta,\gamma)$ of the moving platform. Under the condition that the velocity and initial posture of the CV motor are known, the position vector of point O_2 in the $\{O_1\}$ is $\boldsymbol{O}_2=[x\quad y\quad z]^T$. According to the dimensions of the mechanism and the geometrical relationship among the links, the hinge centre coordinate values in respective coordinate system of four driving limbs can be obtained using vector projection method.

3.1.1. Inverse solution of the HRDL

The position and orientation of the HRDL determines the position and orientation of the HRDM. The link coordinate system of limb *OCDEO'* driven by CV motor are established, as shown in Fig. 3. The coordinate systems {1}-{4} are established at the center of each revolute pair, respectively. z_4-axis of the coordinate system {4} is parallel to

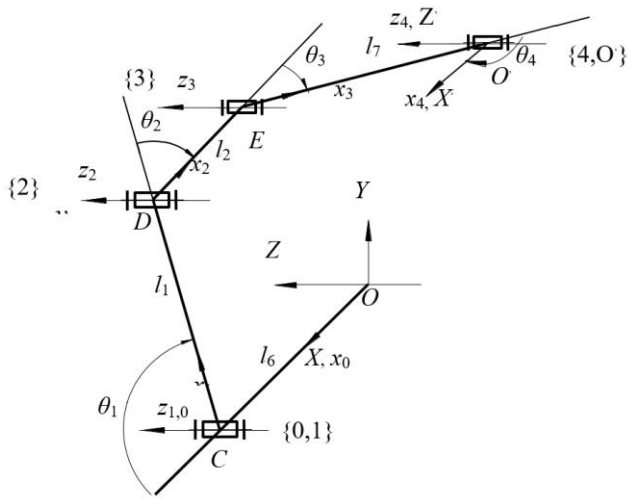

Fig. 3 Link coordinate systems of *OCDEO'*

Table 1

D-H parameters of *OCDEO'* limb

i	a_i	α_i	d_i	θ_i
0	l_6	0	0	0
1	l_1	0	0	θ_1
2	l_2	0	0	θ_2
3	l_7	0	0	θ_3
4	0	0	0	θ_4

Z'-axis of the moving coordinate system {*O'*}. The D-H parameters of *OCDEO'* limb of the HRDL are shown in Table 1.

The kinematics model of the HRDM in the link coordinate systems is established using Denavit-Hartenberg method. The position and orientation of the moving platform of OCDEO' limb can be obtained by homogeneous transformation. The homogeneous transformation matrix from link coordinate system {*i*-1} to link coordinate system {*i*} is ${}^{i}_{i-1}\boldsymbol{T}$, and the general expression of ${}^{i}_{i-1}\boldsymbol{T}$ is

$$ {}^{i}_{i-1}\boldsymbol{T}=\begin{bmatrix} c\theta_i & -s\theta_i c\alpha_i & s\theta_i s\alpha_i & a_i c\theta_i \\ s\theta_i & c\theta_i c\alpha_i & -s\alpha_i & a_i s\theta_i \\ 0 & s\alpha_i & c\alpha_i & d_i \\ 0 & 0 & 0 & 1 \end{bmatrix}. \tag{1} $$

The orientation transformation matrix of the HRDM from the static platform to the moving platform can be expressed as

$$ {}^{O'}_{O}\boldsymbol{T}={}^{0}_{O}\boldsymbol{T}\,{}^{1}_{0}\boldsymbol{T}\,{}^{2}_{1}\boldsymbol{T}\,{}^{3}_{2}\boldsymbol{T}\,{}^{4}_{3}\boldsymbol{T}\,{}^{O'}_{4}\boldsymbol{T}=\begin{bmatrix} m_x & n_x & o_x & x \\ m_y & n_y & o_y & y \\ m_z & n_z & o_z & 0 \\ 0 & 0 & 0 & 1 \end{bmatrix}, \tag{2} $$

where: $m_x = c\theta_{1,2,3,4}$, $m_y = c\theta_{1,2,3,4}$, $m_z = 0$; $n_x = -s\theta_{1,2,3,4}$, $n_y = s\theta_{1,2,3,4}$, $n_z = 0$; $o_x = o_y = 0, o_z = 1$,

$x = l_7 c\theta_{1,2,3} + l_2 c\theta_{1,2} + l_1 c\theta_1 + l_6$,

$y = l_7 s\theta_{1,2,3} + l_2 s\theta_{1,2} + l_1 s\theta_1$.

Here: *s* represents *sin*, *c* represents *cos*, $\theta_{1,2,\cdots,k}$ represents $\theta_1+\theta_2+\cdots+\theta_k$ ($k \in N$).

According to the degrees of freedom characteristics of the HRDM, the position and orientation transformation matrix is obtained by Euler method as follows.

$$ {}^{O'}_{O}\boldsymbol{T}=\begin{bmatrix} \boldsymbol{R} & \boldsymbol{O'} \\ 0 & 1 \end{bmatrix}, \tag{3} $$

where

$\boldsymbol{R}_{zyx}(\alpha,\beta,\gamma)=\left[\begin{bmatrix} c\alpha & -s\alpha & 0 \end{bmatrix},\begin{bmatrix} s\alpha & c\alpha & 0 \end{bmatrix},\begin{bmatrix} 0 & 0 & 1 \end{bmatrix}\right]$ is Euler transformation matrix represented by *Z-Y-X*. $\boldsymbol{O'}=\begin{bmatrix} x & y & 0 \end{bmatrix}^T$ represents the coordinate vector of the origin of the moving coordinate system { O' } in the static coordinate system {*O*}.

Eq. (2) and Eq. (3) are equivalent, and get

$$ \begin{cases} x = l_7 c\theta_{1,2,3} + l_2 c\theta_{1,2} + l_1 c\theta_1 + l_6 \\ y = l_7 s\theta_{1,2,3} + l_2 s\theta_{1,2} + l_1 s\theta_1 \\ z = 0 \\ \beta = \gamma = 0° \\ \alpha = \theta_{1,2,3,4} \end{cases}. \tag{4} $$

Deleting $\theta_{1,2,3}$ from Eq. (4), yield

$$ Ac\theta_{1,2} + Bs\theta_{1,2} + C = 0, \tag{5} $$

where: $A = 2l_2(x - l_1 c\theta_1 - l_6)$, $B = 2l_2(y - l_1 s\theta_1)$,

$C = l_7^2 - l_2^2 - (x - l_1 c\theta_1 - l_6)^2 - (y - l_1 s\theta_1)^2$.

Solving Eq. (5), and obtain

$$ \theta_{1,2} = 2tan^{-1}\left[E(x,y,\alpha)\right], \tag{6} $$

$$ E(x,y,\alpha) = \frac{-B \pm \sqrt{A^2 + B^2 - C^2}}{C - A}, \tag{7} $$

where $E(x,y,\alpha)$ is a function of trajectory $\boldsymbol{X} = [x,y,\alpha]^{\mathrm{T}}$.

For $\theta_{1,2}$ to be continuous, $\dot{\theta}_{1,2}$ must exists. Only when the equation $C - A \neq 0$ holds in the workspace, then Eq. (6) is derivable everywhere. In order for the equation

$$ C - A = -\left[(x - l_1 c\theta_1 - l_6) + l_2\right]^2 - \left[(y - l_1 s\theta_1)^2 - l_7^2\right] \neq 0 $$

to be true everywhere in workspace, as long as

$$ \left\{\left[(x - l_1 c\theta_1 - l_6) + l_2 = 0\right] \& \left[(y - l_1 s\theta_1)^2 - l_7^2 = 0\right]\right\} \neq True $$

is true. Therefore, in trajectory planning, it only needs $y > l_1 + l_7$ to be satisfied.

Similarly, deleting $\theta_{1,2}$ from Eq. (4), yield

$$ \theta_{1,2,3} = 2tan^{-1}\left[F(x,y,\alpha)\right], \tag{8} $$

$$ F(x,y,\alpha) = \frac{-B' \pm \sqrt{A'^2 + B'^2 - C'^2}}{C' - A'}, \tag{9} $$

where: $A' = 2l_7\left(x - l_1 c\theta_1 - l_6\right)$, $B' = 2l_7\left(y - l_1 s\theta_1\right)$,

$C' = l_6^2 - l_7^2 - \left(x - l_1 c\theta_1 - l_6\right)^2 - \left(y - l_1 s\theta_1\right)^2$,

$F\left(x, y, \alpha\right)$ is a function of the trajectory $\boldsymbol{X} = \left[x, y, \alpha\right]^T$.

In order to make Eq. (8) derivable everywhere, it only needs the equation $C' - A' \neq 0$ holds everywhere in the workspace, that is

$$\left\{\left[\left(x - l_1 c\theta_1 - l_6\right) + l_2 = 0\right] \& \left[\left(y - l_1 s\theta_1\right)^2 - l_6^2 = 0\right]\right\} \neq True.$$

It only needs to set $y > l_1 + l_6$ in trajectory planning, thus $\theta_{1,2,3}$ must be continuous everywhere.

Since θ_1 is driven by CV motor, the expression of $\theta_i\ (i = 1, 2, 3, 4)$ is

$$\begin{cases} \theta_1 = \mathrm{C}t + \theta_{10} \\ \theta_2 = \theta_{1,2} - \theta_1 \\ \theta_3 = \theta_{1,2,3} - \theta_{1,2} \\ \theta_4 = \alpha - \theta_{1,2,3} \end{cases}, \tag{10}$$

where, C is the angular velocity of CV motor.

The coordinate vector of point $E\left(x_e, y_e, z_e\right)$ can be obtained by homogeneous transformation

$$^{3}_{O}\boldsymbol{T} = {}^{0}_{O}\boldsymbol{T}\,{}^{1}_{0}\boldsymbol{T}\,{}^{2}_{1}\boldsymbol{T}\,{}^{3}_{2}\boldsymbol{T} = {}^{O'}_{O}\boldsymbol{T}\left({}^{4}_{3}\boldsymbol{T}\,{}^{O'}_{4}\boldsymbol{T}\right)^{-1}. \tag{11}$$

From Eq. (11), the coordinates of point $E\left(x_e, y_e, z_e\right)$ are

$$\begin{cases} x_e = x - l_7 c\left(\alpha - \theta_4\right) \\ y_e = z - l_7 s\left(\alpha - \theta_4\right) \\ z_e = 0 \end{cases}. \tag{12}$$

As shown in Fig. 3, the HRDL works under the coupling of limb *OCEDO'* driven by CV motor and limb *OGFEO'* driven by servo motor. Among them, $\theta_1 = q_1$, $\theta_{1,2} = q_2$. The position and orientation X and q_1 at any time are determined when the HRDM moves in a regular continuous trajectory under the working state. For limb *OCDEO'*, the following vector relation is satisfied.

$$\boldsymbol{O_1E} + \boldsymbol{EO_2} = \boldsymbol{O_1O_2}, \tag{13}$$

$$\boldsymbol{O_1E} = \boldsymbol{O_1C} + \boldsymbol{CD} + \boldsymbol{DE}. \tag{14}$$

There are two solutions satisfying this conditions: points E and E'. At the same time, point E is the coupling point of limb *OCDE* and limb *OGFE*, thus the following conditions should also be satisfied.

$$\boldsymbol{O_1E} = \boldsymbol{O_1G} + \boldsymbol{GF} + \boldsymbol{FE}. \tag{15}$$

From Fig. 3, if both points E and E' can satisfy the geometric constraints of the servo drive limb, there must be $|\boldsymbol{FE}| = |\boldsymbol{FE'}|$, $|\boldsymbol{DE}| = |\boldsymbol{DE'}|$, at this time, $\boldsymbol{\Delta FED} \cong \boldsymbol{\Delta FE'D}$. It is further obtained that points E and E' are coincide, but this contradicts the fact point E and point E' are two different points. Therefore, point E is unique that can satisfy the constraints of two driving limbs simultaneously. According to the assembly relationship of the five-bar mechanism *CDEFG*, y_e is located above the *XOZ* plane.

$$\begin{aligned} &|\boldsymbol{FG} - \boldsymbol{EF}| \le |\boldsymbol{O_1E}| \le |\boldsymbol{FG}| + |\boldsymbol{EF}| \\ &|\boldsymbol{CD} - \boldsymbol{DE}| \le |\boldsymbol{O_1E}| \le |\boldsymbol{CD}| + |\boldsymbol{DE}| \end{aligned}. \tag{16}$$

If the vector Eq. (14) and Eq. (15) are projected to X axis and Y axis respectively, the trajectory of point E is a function about the input angular displacement q_1 of CV motor and the input angular displacement q_4 of servo motor, which is obtained using trigonometric function relationship.

$$\begin{cases} x_e = f\left(q_1, q_4\right) = l_6 + l_1 c\,q_1 + l_2 c\,q_2\left(q_1, q_4\right) \\ \quad = -l_5 + l_4 c\,q_4 + l_3 c\,q_3\left(q_1, q_4\right) \\ y_e = g\left(q_1, q_4\right) = l_1 s\,q_1 + l_2 s\,q_2\left(q_1, q_4\right) \\ \quad = l_4 s\,q_4 + l_3 s\,q_3\left(q_1, q_4\right) \end{cases}. \tag{17}$$

From Eq. (17), the relationship of included angles q_2, q_3 of the links with respect to E point coordinate vector, the angular displacements q_1 of CV motor and q_4 of serve motor can be obtained

$$\begin{cases} q_2 = tan^{-1}\left(\dfrac{y_e - l_1 s q_1}{x - l_1 c q_1 - l_5}\right) \\ q_3 = tan^{-1}\left(\dfrac{y_e - l_1 s q_4}{x - l_4 c q_4 - l_6}\right) \end{cases}, \tag{18}$$

where, the angular displacement $q_1 = \theta_1$ of CV motor is known, thus q_2 is uniquely determined. q_3 will be determined with the driving angular displacement q_4 of servo motor.

Eliminating q_2 and q_3 from Eq. (17), yield

$$\begin{cases} \left(x_e - l_1 c\,q_1 - l_6\right)^2 + \left(y_e - l_1 s q_1\right)^2 = l_2^2 \\ \left(x_e - l_4 c\,q_4 + l_5\right)^2 + \left(y_e - l_4 s q_4\right)^2 = l_3^2 \end{cases}. \tag{19}$$

Rearranging it as function of q_1 and q_4, yield

$$\begin{cases} L_3 + M_3 c\,q_1 + N_3 s q_1 = 0 \\ L_4 + M_4 c\,q_4 + N_4 s q_4 = 0 \end{cases}, \tag{20}$$

where:

$$\begin{cases} L_3 = \left(x_e - l_6\right)^2 + l_1^2 - l_2^2 + {y_e}^2 \\ M_3 = -2l_1\left(x_e - l_6\right) \\ N_3 = -2l_1 y_e \end{cases}, \begin{cases} L_4 = \left(x_e + l_5\right)^2 + l_4^2 - l_3^2 + {y_e}^2 \\ M_4 = -2l_4\left(x_e + l_5\right) \\ N_4 = -2l_4 y_e \end{cases}.$$

Using half-angle formula of trigonometric function to solve Eq. (20), the following solutions are obtained

$$\begin{cases} q_1 = 2\,tan^{-1}\left[G\left(x, y, \alpha\right)\right] \\ q_4 = 2\,tan^{-1}\left[H\left(x, y, \alpha\right)\right] \end{cases}, \tag{21}$$

where:

$$G(x,y,\alpha)=\frac{N_3\pm\sqrt{N_3^2+M_3^2-L_3^2}}{L_3-M_3}, \tag{22}$$

$$H(x,y,\alpha)=\frac{N_4\pm\sqrt{N_4^2+M_4^2-L_4^2}}{L_4-M_4}. \tag{23}$$

Eq. (21) and Eq. (18) is the inverse solution of the HRDL. Because q_1 and q_2 are uniquely determined, q_4 is a function about $H(x,y,\alpha)$. According to Eq. (21) and Eq. (22), there are two compensation angles of servo motor theoretically, and the expression is

$$q_4=H_1(X)=tan\left(\frac{N_4+\sqrt{N_4^2+M_4^2-L_4^2}}{L_4-M_4}\right)^{-1},$$

$$q_4'=H_1'(X)=tan\left(\frac{N_4-\sqrt{N_4^2+M_4^2-L_4^2}}{L_4-M_4}\right)^{-1}.$$

When $L_4-M_4\neq 0$ is satisfied, that is,

$$\left\{\left[\left(x_e+l_5\right)^2-l_4^2=0\right]\&\left[y_e^2-l_3^2=0\right]\right\}\neq True.$$

$H(X)$ and $H'(X)$ are differentiable everywhere in the workspace Ω. Thus, q_4 and q_4' is continuous in the workspace Ω. Therefore, q_4, q_4' are continuous and exists everywhere. When the initial position and orientation X_0 of the HRDM and the angular displacement q_1 of CV motor are determined, in order to make the HRDM work normally, an angle must be selected from the corresponding q_4 and q_4' as the initial compensation angle of servo motor.

Setting q_4 as the initial compensation angle of serve motor, it is always a function of $H_1(X)$. To keep q_4 the continuity of q_4, only $H_1'(X)$ exist. In fact, $H_1(X)$ is differentiable everywhere in the workspace Ω. q_4 is then determined and is unique. q_3 is determined by q_4. Therefore, once the initial configuration of the HRDM is determined, to maintain the continuity of the inverse solution of the HRDL, and the existence of $q_i\,(i=1,2,3,4)$ is continuous and unique.

3.1.2. The inverse position solution of 3-PSS limb

According to dimension parameters of the HRDM, the coordinate vector of $B_i, S_i\,(i=1,2,3)$ in the static coordinate system is obtained, respectively. The coordinate vector of point Pi in moving coordinate expressed as ${}^{O'}P_i\,(i=1,2,3)$. The coordinate vector $\boldsymbol{P_i}\,(i=1,2,3)$ in the static coordinate system can be expressed as

$$\boldsymbol{P_i}=\boldsymbol{R}\,{}^{O'}\boldsymbol{P_i}+\boldsymbol{O'}\,(i=1,2,3). \tag{24}$$

The vector equation of the *i*-th PSS limb is obtained by closed vector method

$$\boldsymbol{OB_i}+\boldsymbol{B_iS_i}=\boldsymbol{OS_i}, \tag{25}$$

$$\boldsymbol{OS_i}+\boldsymbol{S_iP_i}=\boldsymbol{OP_i}, \tag{26}$$

$$\left|\boldsymbol{S_iP_i}\right|=\boldsymbol{L_i}, \tag{27}$$

$$\boldsymbol{h_i}=\left|\boldsymbol{B_iS_i}\right|, \tag{28}$$

where: L_i (*i*=1, 2, 3) is the link length of *i*-th PSS limb; $\boldsymbol{h_i}$ represents the driving displacement of the prismatic pair $\boldsymbol{S_i}$. Eq. (28) is the position inverse solution of 3-PSS limb.

3.2. Velocity analysis of 3-PSS/7R HRDM

Jacobian matrix represents corresponding relationship between generalized velocity vector of three prismatic pairs and generalized velocity of the moving platform. Jacobian mapping matrix of the HRDM is a non-full rank matrix, which has 5 motion inputs but only 3 motion outputs, and can be expressed as following relationship.

$$\dot{\boldsymbol{Q}}=\boldsymbol{J}\dot{\boldsymbol{X}}, \tag{29}$$

where, $\dot{\boldsymbol{X}}=\left(\dot{x},\dot{z},\dot{\beta}\right)^T$ is the generalized output velocity vector of the center of the moving platform. $\dot{\boldsymbol{Q}}=\left[\dot{q}_1,\dot{q}_4,\dot{h}_1,\dot{h}_2,\dot{h}_3\right]^T$ is the driving velocity vector of the generalized joint.

3.2.1. Velocity analysis of the HRDL

Driven by CV motor and servo motor, the hybrid motion input generates coupling velocity at point *E* through the coupling action of the parallel five-bar mechanism, and then transmits motion to the center of the moving platform through the spatial link *EO'*, so as to output a flexible and controllable trajectory. The velocity of the HRDL satisfies the following relationship.

$$\dot{\boldsymbol{Q}}_1={}^1\boldsymbol{J}\dot{\boldsymbol{X}}, \tag{30}$$

where, $\dot{\boldsymbol{Q}}_1=\left(\dot{q}_1,\dot{q}_4\right)^T$ is the velocity of CV motor and servo motor, respectively. ${}^1\boldsymbol{J}$ is the Jacobian matrix of the HRDL.

Taking the derivative of Eq. (17) with respect to time and considering the coupling between servo motor drive and CV motor drive, the mapping relationship between the input velocity and the velocity of the coupling point E is obtained.

$$\dot{\boldsymbol{Q}}_1={}_1^1\boldsymbol{J}\dot{\boldsymbol{l}}_e, \tag{31}$$

where

$${}_1^1\boldsymbol{J}=\left[\begin{bmatrix}{}_1^1j_{11} & {}_1^1j_{12}\end{bmatrix},\begin{bmatrix}{}_1^1j_{21} & {}_1^1j_{22}\end{bmatrix}\right], \tag{32}$$

where:

$${}_1^1j_{11}=s\left(q_2-q_3\right)\left[-l_1sq_1s\left(q_2-q_3\right)+l_1sq_2s\left(q_1-q_3\right)\right]^{-1},$$

$${}_1^1j_{12}=-l_4sq_2s\left(q_2-q_3\right)s\left(q_4-q_3\right)^{-1},$$

$${}_1^1j_{21} = s(q_2 - q_3)\left[l_1cq_1s(q_2 - q_3) - l_1cq_2s(q_1 - q_3)\right],$$

$${}_1^1j_{22} = l_4cq_2s(q_2 - q_3)s(q_4 - q_3).$$

At any instant, the velocity relation between the coupling point *E* of the HRDL and the moving platform satisfies

$$\dot{\boldsymbol{l}}_e = {}_2^1\boldsymbol{J}\dot{\boldsymbol{X}}. \tag{33}$$

Taking the derivative of Eq. (12) with respect to time, yield

$$\begin{cases} \dot{x}_e = \dot{x} + l_7s(\alpha - \theta_4)(\dot{\alpha} - \dot{\theta}_4) \\ \dot{y}_e = \dot{y} - l_7c(\alpha - \theta_4)(\dot{\alpha} - \dot{\theta}_4) \end{cases}. \tag{34}$$

According to Eq. (6) and Eq. (9), $E(x,y,\alpha)$ and $F(x,y,\alpha)$ are functions about X, which are continuous in the workspace and derivable everywhere.

Taking the derivative of Eq. (10) with respect time, yield

$$\begin{cases} \dot{\theta}_1 = C \\ \dot{\theta}_2 = \dfrac{2}{1+E^2}\left[\dfrac{\partial E}{\partial x} \quad \dfrac{\partial E}{\partial y} \quad \dfrac{\partial E}{\partial \alpha}\right]\cdot\dot{X} - C \\ \dot{\theta}_3 = \left(\dfrac{2}{1+F^2} - \dfrac{2}{1+E^2}\right)\bullet \\ \quad \bullet\left[\dfrac{\partial F}{\partial x} - \dfrac{\partial E}{\partial x} \quad \dfrac{\partial F}{\partial y} - \dfrac{\partial E}{\partial y} \quad \dfrac{\partial F}{\partial \alpha} - \dfrac{\partial E}{\partial \alpha}\right]\dot{X} + C \\ \dot{\theta}_4 = \left[\dfrac{-2}{1+F^2}\dfrac{\partial F}{\partial x} \quad \dfrac{-2}{1+F^2}\dfrac{\partial F}{\partial y} \quad 1 - \dfrac{2}{1+F^2}\dfrac{\partial F}{\partial \alpha}\right]\cdot\dot{X} \end{cases}. \tag{35}$$

Substituting Eq. (35) into Eq. (34), and get

$${}_2^1\boldsymbol{J} = \left[\left[{}_2^1j_{11} \quad {}_2^1j_{12} \quad {}_2^1j_{13}\right], \left[{}_2^1j_{21} \quad {}_2^1j_{22} \quad {}_2^1j_{23}\right]\right], \tag{36}$$

where:

$${}_2^1j_{11} = 1 + \frac{2l_7s(\alpha - \theta_4)}{1+F^2}\frac{\partial F}{\partial x},\ {}_2^1j_{12} = \frac{2l_7s(\alpha - \theta_4)}{1+F^2}\frac{\partial F}{\partial y};$$

$${}_2^1j_{13} = \frac{2l_7s(\alpha - \theta_4)}{1+F^2}\frac{\partial F}{\partial \alpha},\ {}_2^1j_{21} = 1 + \frac{2l_7c(\alpha - \theta_4)}{1+F^2}\frac{\partial F}{\partial x};$$

$${}_2^1j_{12} = 1 + \frac{2l_7c(\alpha - \theta_4)}{1+F^2}\frac{\partial F}{\partial y},\ {}_2^1j_{13} = -\frac{2l_7c(\alpha - \theta_4)}{1+F^2}\frac{\partial F}{\partial \alpha}.$$

To sum up,

$${}^1\boldsymbol{J} = {}_1^1\boldsymbol{J}\cdot{}_2^1\boldsymbol{J}. \tag{37}$$

3.2.2. Velocity of 3-PSS limb

The Jacobian matrix of 3-PSS limb can be obtained by calculating the first derivative of Eq. (5) with respect to time, get

$$\dot{\boldsymbol{Q}}_2 = {}^2\boldsymbol{J}\dot{\boldsymbol{X}}, \tag{38}$$

where, $\dot{\boldsymbol{Q}}_2 = \left[\dot{h}_1 \quad \dot{h}_2 \quad \dot{h}_3\right]^T$ is the driving velocity of the prismatic pairs of 3-PSS limb.

$${}^2\boldsymbol{J} = \left[\left[{}^2j_1\right] \quad \left[{}^2j_2\right] \quad \left[{}^2j_3\right]\right]^T, \tag{39}$$

where, $\left[{}^2j_i\right] = \left[\dfrac{\partial h_i}{\partial x} \quad \dfrac{\partial h_i}{\partial y} \quad \dfrac{\partial h_i}{\partial \alpha}\right]^{\mathrm{T}}$, $(i = 1,2,3)$.

Then the overall Jacobian matrix of 3-PSS/7R HRDM is expressed as

$${}^1\boldsymbol{J} = \left[{}^1\boldsymbol{J} \quad {}^2\boldsymbol{J}\right]^T. \tag{40}$$

3.3. Acceleration analysis of the HRDM

3.3.1. Acceleration of the HRDL

The acceleration is analyzed on the basis of inverse kinematics analysis and velocity analysis of the HRDL. Taking the derivative of Eq. (30) with respect to time, get.

$$\ddot{\boldsymbol{Q}}_1 = {}^1\boldsymbol{J}\dot{\boldsymbol{X}} + {}^1\boldsymbol{J}\ddot{\boldsymbol{X}}, \tag{41}$$

where, $\ddot{\boldsymbol{Q}}_1 = \left(\ddot{q}_1, \ddot{q}_4\right)^T$ is the driving acceleration of the HRDL.

In order to obtain ${}^1\dot{\boldsymbol{J}}$, taking the derivative of Eq. (37) further with respect to time, get

$${}^1\dot{\boldsymbol{J}} = {}_1^1\dot{\boldsymbol{J}}\cdot{}_2^1\boldsymbol{J} + {}_1^1\boldsymbol{J}\cdot{}_2^1\dot{\boldsymbol{J}}, \tag{42}$$

$${}_1^1\dot{\boldsymbol{J}} = \begin{bmatrix} {}_1^1\dot{j}_{11} & {}_1^1\dot{j}_{12} \\ {}_1^1\dot{j}_{21} & {}_1^1\dot{j}_{22} \end{bmatrix}, \tag{43}$$

where,

$${}_1^1\dot{j}_{ij} = \frac{\partial\left({}_1^1\boldsymbol{j}_{ij}\right)}{\partial q_1}\dot{q}_1 + \frac{\partial\left({}_1^1\boldsymbol{j}_{ij}\right)}{\partial q_2}\dot{q}_2 + \frac{\partial\left({}_1^1\boldsymbol{j}_{ij}\right)}{\partial q_3}\dot{q}_4 + \frac{\partial\left({}_1^1\boldsymbol{j}_{ij}\right)}{\partial q_4}\dot{q}_4\ (i,j = 1,2),$$

$${}_2^1\dot{\boldsymbol{J}} = \begin{bmatrix} {}_2^1\dot{j}_{11} & {}_2^1\dot{j}_{12} & {}_2^1\dot{j}_{13} \\ {}_2^1\dot{j}_{21} & {}_2^1\dot{j}_{22} & {}_2^1\dot{j}_{23} \end{bmatrix}, \tag{44}$$

where:

$${}_2^1\dot{j}_{11} = \frac{\partial\left({}_2^1j_{11}\right)}{\partial x} + \frac{\partial\left({}_2^1j_{11}\right)}{\partial y} + \frac{\partial\left({}_2^1j_{11}\right)}{\partial \alpha},$$

$${}_2^1\dot{j}_{12} = \frac{\partial\left({}_2^1j_{12}\right)}{\partial x} + \frac{\partial\left({}_2^1j_{12}\right)}{\partial y} + \frac{\partial\left({}_2^1j_{12}\right)}{\partial \alpha},$$

$${}_2^1\dot{j}_{13} = \frac{\partial\left({}_2^1j_{13}\right)}{\partial x} + \frac{\partial\left({}_2^1j_{13}\right)}{\partial y} + \frac{\partial\left({}_2^1j_{13}\right)}{\partial \alpha},$$

$${}_2^1\dot{j}_{21} = \frac{\partial\left({}_2^1j_{21}\right)}{\partial x} + \frac{\partial\left({}_2^1j_{21}\right)}{\partial y} + \frac{\partial\left({}_2^1j_{21}\right)}{\partial \alpha},$$

$$
{}_2^1\dot{j}_{12} = \frac{\partial\left({}_2^1 j_{22}\right)}{\partial x} + \frac{\partial\left({}_2^1 j_{22}\right)}{\partial y} + \frac{\partial\left({}_2^1 j_{22}\right)}{\partial \alpha},
$$

$$
{}_2^1\dot{j}_{13} = \frac{\partial\left({}_2^1 j_{23}\right)}{\partial x} + \frac{\partial\left({}_2^1 j_{23}\right)}{\partial y} + \frac{\partial\left({}_2^1 j_{23}\right)}{\partial \alpha}.
$$

Eq. (41) is the acceleration array of the HRDL. Thus, the acceleration array at the center of the moving platform can be further calculated.

3.3.2. Acceleration of 3-PSS limb

The acceleration is analyzed on the basis of the position analysis and velocity analysis. Taking the derivative of Eq. (38) with respect to time, and then obtain

$$
\ddot{\boldsymbol{Q}}_2 = {}^2\boldsymbol{J}\dot{\boldsymbol{X}} + {}^2\dot{\boldsymbol{J}}\ddot{\boldsymbol{X}}, \tag{45}
$$

where $\ddot{\boldsymbol{Q}}_2 = \begin{bmatrix} \ddot{h}_1 & \ddot{h}_2 & \ddot{h}_3 \end{bmatrix}^T$ is the driving acceleration of the prismatic pairs of 3-PSS limb.

$$
{}^2\dot{\boldsymbol{J}} = \left[\begin{bmatrix} {}^2\dot{j}_1 \end{bmatrix} \quad \begin{bmatrix} {}^2\dot{j}_2 \end{bmatrix} \quad \begin{bmatrix} {}^2\dot{j}_3 \end{bmatrix}\right]^T, \tag{46}
$$

where:

$$
\begin{bmatrix} {}^2\dot{j}_i \end{bmatrix} = \begin{bmatrix} {}^2\dot{j}_{i1} & {}^2\dot{j}_{i2} & {}^2\dot{j}_{i3} \end{bmatrix}^T, \ (i = 1,2,3),
$$

$$
{}^2\dot{j}_{i1} = \frac{\partial^2 h_i}{\partial^2 x} + \frac{\partial^2 h_i}{\partial x \partial y} + \frac{\partial^2 h_i}{\partial x \partial \alpha},
$$

$$
{}^2\dot{j}_{i2} = \frac{\partial^2 h_i}{\partial x \partial y} + \frac{\partial^2 h_i}{\partial^2 y} + \frac{\partial^2 h_i}{\partial y \partial \alpha},
$$

$$
{}^2\dot{j}_{i3} = \frac{\partial^2 h_i}{\partial x \partial \alpha} + \frac{\partial^2 h_i}{\partial y \partial \alpha} + \frac{\partial^2 h_i}{\partial^2 \alpha}.
$$

Eq. (45) is the acceleration array of 3-PSS limb.

4. Continuity condition of motion trajectory of the HRDM

4.1. Requirements for servo motor of the HRDL to realize smooth trajectory of the moving platform center

The 3-PSS limb does not constrain the DOFs of the HRDM and does not affect the trajectory of the moving platform in reachable workspace of the HRDM. Therefore, in order to study the trajectory smoothness of the moving platform, it is only necessary to study the trajectory smoothness of the HRDL end. For the trajectory *X* of the center of the moving platform, the necessary condition for its trajectory continuity is $\dot{\boldsymbol{X}}(t)$ continuity. The HRDL is coupled at point *E*. $\dot{\boldsymbol{X}}(t)$ and the velocities of point *E* have following relationship.

$$
\dot{\boldsymbol{X}}(t) = \left[\left(\partial \boldsymbol{X}\right) / \left(\partial \boldsymbol{l}_e\right)\right]\dot{\boldsymbol{l}}_e = {}_2^1\boldsymbol{J}^{-1}\dot{\boldsymbol{l}}_e. \tag{47}
$$

From Section 3, as long as the size parameters of the HRDM are properly designed, ${}_2^1\boldsymbol{J}$ exists everywhere, thus $\dot{\boldsymbol{l}}_e$ is continuous.

At the same time, the trajectory of point *E* is generated by the joint action of CV motor and servo motor. The necessary condition for continuous trajectory of point E is that $\dot{x}_e(t)$ and $\dot{y}_e(t)$ are continuous and get

$$
\left[\dot{x}_e(t)\right]^2 + \left[\dot{y}_e(t)\right]^2 \neq 0. \tag{48}
$$

Since the trajectory *X* is located above *XOZ* , Eq. (48) is always valid.

By differentiating Eq. (17) with respect to time, the functions of $\dot{\boldsymbol{l}}_e$ about driving velocity of CV motor and servo motor can be obtained.

$$
\begin{cases} \dot{x}_e(t) = \dfrac{\partial f}{\partial q_1} C + \dfrac{\partial f}{\partial q_1}\dot{q}_4 \\ \dot{y}_e(t) = \dfrac{\partial g}{\partial q_4} C + \dfrac{\partial g}{\partial q_4}\dot{q}_4 \end{cases}, \tag{49}
$$

where $\partial f / \partial q_1$ represents derivative of horizontal displacement x of the coupling point E to the angular displacement q_1 of CV motor when the velocity of servo motor is 0.

Since the trajectory of point E is equivalent to end trajectory of the four-bar linkage *GFED*, $\partial f / \partial q_1$ must be continuous. Similarly, the derived functions $\partial f / \partial q_4$, $\partial f / \partial q_1$ and $\partial f / \partial q_4$ are also continuous. Therefore, the velocity function $\dot{q}_4(t)$ of servo motor determines the smoothness of the moving platform of the HRDL. If $\dot{q}_4(t)$ is continuous, the trajectory of the moving platform is smooth curve. If it is discontinuous or does not exist, $\dot{\boldsymbol{X}}(t)$ is discontinuous. At this time, the trajectory of the moving platform is continuous but not a smooth curve.

In conclusion, the sufficient and necessary conditions for smooth trajectories of the moving platform of the HRDM is that derivative of servo motor motion input function is continuous. That is, the driving velocity of servo motor has no step.

4.2. Trajectory planning of the HRDM

In the full servo parallel mechanism, the driving angle of each servo motor can rotate in both directions, and any trajectory in the workspace can be realized theoretically. The motion input of the HRDM is essentially different from it, due to the existence of CV motor. Once the initial angular displacement, angular velocity and direction of CV motor are set, the mechanism cannot realize any trajectory in the workspace on the same configuration and parameters. Only when the trajectory curve satisfies the properties of unidirectional constant velocity driven by CV motor and the constraint conditions of the HRDL, the trajectory curve can be reproduced in the HRDM.

In order to make the HRDM realize trajectory in the workspace, it is necessary to plan the trajectory of the mechanism. The HRDL determines the DOFs of the HRDM. In trajectory planning, as long as the planned trajectory can be realized at the end of the HRDL, the whole mechanism can realize planned trajectory. Therefore, the trajectory planning problem of the HRDM moving platform

is transformed into the trajectory planning problem of the HRDL. Under the working state of the HRDL, the driving angular displacement $\boldsymbol{q}_1(t)=\boldsymbol{\theta}_1(t)$ of CV motor is determined at any time t. At this time, the reachable region of the end point of the mechanism can be regarded as the curve cluster formed by the trajectory $\boldsymbol{X}(t)$ of point $\boldsymbol{O}'$, which is expressed as

$$\begin{cases} x(t)=m_1(q_1,q_4)\big|_{q_1=Ct} \\ y(t)=m_2(q_1,q_4)\big|_{q_1=Ct} \\ \alpha(t)=m_3(q_1,q_4)\big|_{q_1=Ct} \end{cases}, \quad t\in[0,t_d], \tag{50}$$

where, t is time variable, t_d is termination time of CV motor input.

4.3. Necessary and sufficient conditions for the HRDM to realize continuous trajectory

For the theoretical trajectory function to be reproduced by the HRDM, its expression is defined as

$$\begin{cases} x=\varphi_1(T) \\ y=\varphi_2(T) \\ \alpha=\varphi_3(T) \end{cases}, \quad T\in[0,T_d], \tag{51}$$

where, T is the equivalent time parameter of the reproduction trajectory, and T_d is the duration of the reproduction trajectory.

In order to reproduce the theoretical trajectory, the driving function of CV motor can be expressed as

$$q_1(t)=q_{10}+\frac{q_d-q_{10}}{T}t=q_{10}+Ct, \quad t\in[0,T_d], \tag{52}$$

where, q_{10} is the initial angular displacement of CV motor, q_d is the end angular displacement of CV motor, and C is the input angular velocity of CV motor.

The driving function of CV input is determined by Eq. (52). The actual running trajectory of the center of the moving platform of the HRDM can be expressed as

$$\begin{cases} x(t)=m_1(q_1,q_4)\big|_{q_1=q_1(t)} \\ y(t)=m_2(q_1,q_4)\big|_{q_1=q_1(t)} \\ \alpha(t)=m_3(q_1,q_4)\big|_{q_1=q_1(t)} \end{cases}, \quad t\in[0,t_d]. \tag{53}$$

Assuming that the given theoretical trajectory to be planned can be stably realized at the end of the HRDL, in the actual trajectory Eq. (53) of the point O'' at any time T, there is time t, so that the end trajectory curve passes through point O''. That is, the function $T=\Phi(t)$ exists. where, T is the equivalent time parameter. t is the time variable of the CV motor drive function.

The equation $T=\Phi(t)$ represents the relationship between the trajectory position and the driving angular displacement when the HRDM reproduces the given trajectory. Therefore, $T=\Phi(t)$ is also called the equation of the position deviation.

The theoretical trajectory point P_T at time T corresponds to the actual trajectory point P_t expressed by Eq. (53) at time t. Assuming that the theoretical trajectory point P_T' at time $T+\Delta T$ ($\Delta T>0$) corresponds to the actual trajectory P_t' at time $t+\Delta t$ ($\Delta t>0$), in order to make the HRDL reproduce the continuous trajectory, P_T corresponds to P_t one by one in the whole working cycle, and ΔT must be greater than zero.

$$\phi(t)=\frac{\phi(t+\Delta t)-\phi(t)}{t+\Delta t-t}=\frac{\Delta T}{\Delta t}>0. \tag{54}$$

Obviously, the position equation $T=\Phi(t)$ is a monotone function. According to the above analysis, the necessary and sufficient condition for the HRDM to reproduce trajectory is that the position equation $T=\Phi(t)$ exists and is a monotone function.

5. Kinematic analysis examples of the HRDM

In order to verify the continuity and uniqueness of the inverse kinematics position solution of 3-PSS/7R HRDM and joint points of each revolute pair of the HRDL, when planned trajectory X, given q_1 and initial configuration of the HRDL are determined, assuming that in the HRDL, the angular velocity of CV motor is $\dot{q}_1=24°/s$, the initial angular displacement is $q_{10}=0$, and the time of CV motor running for one cycle is 15 s, the movement law of the center of the moving platform is defined as

$$\begin{cases} x=20\sin(2\pi\cdot t/15) \\ y=20\cos(2\pi\cdot t/15), \quad (0\le t\le 15) \\ \alpha=\begin{cases} 2t/3, & (0\le t\le 7.5) \\ 10-2t/3, & (7.5\le t\le 15) \end{cases} \end{cases}. \tag{55}$$

Based on the position inverse solution Eq. (28) of the HRDM, the displacement variations of the prismatic pairs of 3-PSS limb are shown in Fig. 4. The displacement curves of point E can be obtained by Eq. (12) are shown in Fig. 5. The variations of the angular displacement q_i(i =2, 3, 4) are shown in Fig. 6. The driving velocity variations of 3-PSS limb can be obtained from the inverse velocity solution Eq. (38), as shown in Fig. 7.

The velocity variations at point E are shown in Fig. 8. The variation of the compensation angular velocity $\dot{\boldsymbol{q}}_4$ of servo motor and the variations of the angular velocities $\dot{\boldsymbol{q}}_2,\dot{\boldsymbol{q}}_3$ of the included angles of links are shown in Fig. 9. Similarly, the driving acceleration variations of the prismatic pairs of 3-PSS limb are shown in Fig. 10. The variations of the acceleration of the coupling point E are shown in Fig. 11.

The variations of the compensation angular acceleration $\ddot{q}_4$ and the angular acceleration $\ddot{q}_2,\ddot{q}_3$ of the included angles of links are shown in Fig. 12.

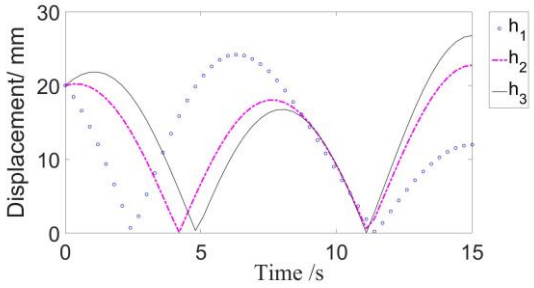

Fig. 4 The variations of the displacements of 3-PSS driving sliders

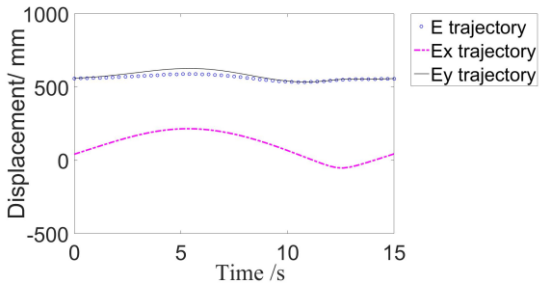

Fig. 5 The variations of the displacements of point *E*

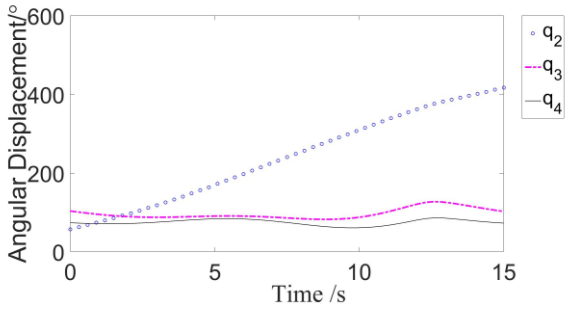

Fig. 6 The variations of the angular displacements $q_i (i = 2, 3, 4)$

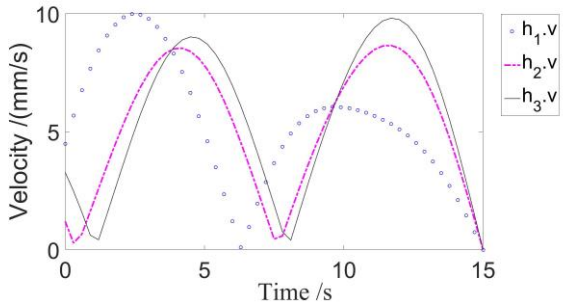

Fig. 7 The variations of the velocities of 3-PSS driving sliders

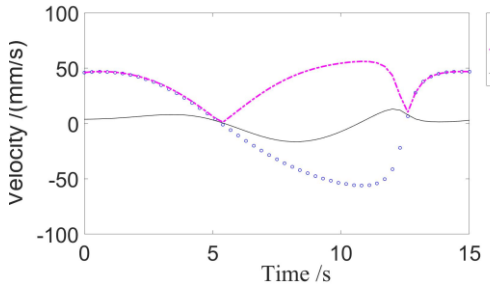

Fig. 8 The variations of the velocities of point *E*

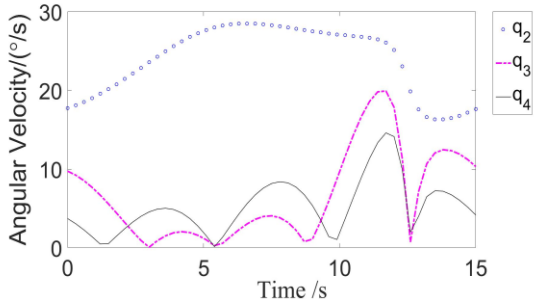

Fig. 9 The variations of the angular velocities $\dot{q}_i \left(i = 2, 3, 4\right)$

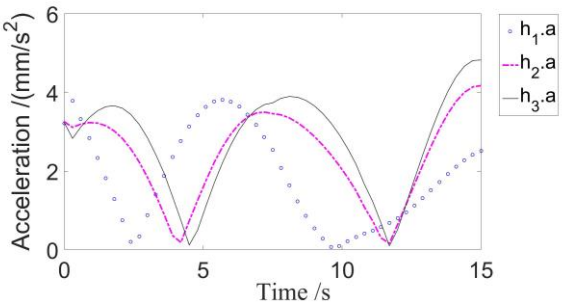

Fig. 10 The variations of the accelerations of PSS

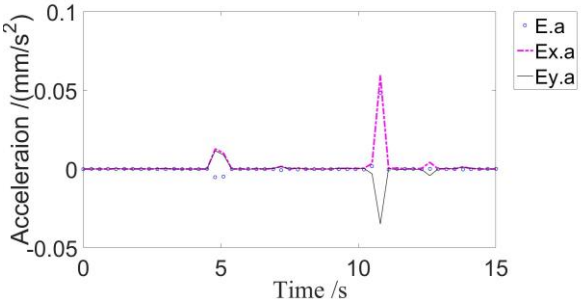

Fig. 11 The variations of the accelerations of point *E*

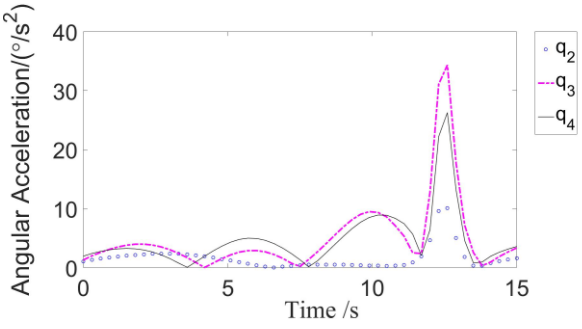

Fig. 12 The variations of the angular accelerations $\ddot{q}_i \left(i = 2, 3, 4\right)$

The planned trajectory X of the center of the moving platform is coherent and smooth. The following conclusions can be obtained by analyzing the kinematic variations in Fig. 4 - Fig. 12.

The inverse solutions $\dot{h}_i \left(i = 1, 2, 3\right)$ and $\dot{q}_4$ of the HRDM are unique with the determination of the driving angular displacement q_{40} of servo motor.

The variations of the displacements and velocities of the coupling point *E* are gentle and continuous without jump. There is a small jump in acceleration curve, but they

are still continuous and smooth, which does not affect the stability of the mechanism operation.

The variations of the displacement h_i and the velocity $\dot{h}_i$ of 3-PSS limb, and the angular displacement q_4 and angular velocity $\dot{q}_4$ are all smooth and coherent. The correctness of Eq. (47) is proved. The smoothness of $\dot{q}_4$ ensures the smoothness of the *X* trajectory of the moving platform of the mechanism. At the same time, the variations of the curves $\ddot{h}_i$ and $\ddot{q}_4$ are smooth without jump, which ensure smooth operation and overall controllability of the mechanism.

The variation of the angular velocity $\dot{q}_i\,(i=2,3,4)$ of the HRDL is consistent, which confirms that the position inverse solution is differentiable in the workspace, and further verifies the continuity and uniqueness of the inverse solution of the HRDM. The variation of the curve $\ddot{q}_i\,(i=2,3,4)$ is smooth with a small change range, and the servo motor will not be greatly impacted. Therefore, the HRDL is also stable and controllable.

6. Conclusions

3-PSS/7R HRDM with the characteristics of both hybrid-driven mechanism and redundantly driven mechanism is studied. The position inverse solution equations of the symmetric limbs and the HRDL are established based on vector method, respectively. Based on it, the velocities and accelerations of the HRDM are analyzed. In this process, the inverse kinematics solution is unique with determination of the angular displacement of CV motor and initial compensation displacement of servo motor of the HRDL.

Further, the sufficient and necessary conditions for the center of the moving platform to realize smooth trajectory are studied. And the sufficient and necessary conditions for reproducing planning trajectory of the HRDM are also studied. Finally, an example is given to verify the correctness of the kinematic theoretical model.

The variations of the displacement curves, velocity curves and acceleration curves of the motion input are smooth, continuous and without large step. The overall operation of the HRDM is stable and controllable. The research results in this study lay a foundation for the research on dynamics, control system and application of the spatial hybrid-driven mechanism.

Acknowledgements

This work is supported by the Key Research and Development Program of Shanxi Province of China (International Cooperation, Nos. 201803D421027, 201903D421051), and the Key Research and Development Program of Shanxi Province of China (No. 202202150401018), the Opening Foundation of Shanxi Key Laboratory of Advanced Manufacturing Technology (No. XJZZ202302).

References

1. **Tokuz, L. C.** 1992. Hybrid machine modelling and control, Ph.D. thesis, Liverpool Polytechnic, UK.
2. **Dülger, L. C.; Kireçci, A.; Topalbekroglu, M.** 2003. Modeling and simulation of a hybrid actuator, Mechanism and Machine Theory 38: 395-407. https://doi.org/10.1016/S0094-114X(02)00129-5.
3. **Kütük, M. E.; Dülger, L. C.** 2016. A hybrid press system: motion design and inverse kinematics issues, Engineering Science and Technology, an International Journal 19: 846-856. https://doi.org/10.1016/j.jestch.2015.11.012.
4. **Dang, X. Z.; Zhou, L. S.; Liang, D.** (2013). Dynamic performance analysis and simulation of hybrid-driven seven-bar mechanical press with double cranks. Advanced Materials Research, 834-836, 1327-1332. https://doi.org/10.4028/www.scientific.net/AMR.834-836.1327.
5. **Gong, J.; Wang, X.; Huang, F; Zhang, Y.** 2015. Dynamic performances analysis of hybrid press based on dependent generalized coordinates, Proceedings of the Institution of Mechanical Engineers, Part C: Journal of Mechanical Engineering Science 229(12): 2187-2194. https://doi.org/10.1177/0954406214557342.
6. **Tso, P. L.** 2010. Optimal design of a hybrid-driven servo press and experimental verification, ASME Journal of Mechanical Design 132: 034503_1-4. https://doi.org/10.1115/1.4000213.
7. **Li, H.; Zhang, Y., H. Zheng.**2008. Dynamics modeling and simulation of a new nine-bar press with hybrid-driven mechanism, J Mech Sci Technol 22(12) 2436-2444. https://doi.org/ 10.1007/s12206-008-0803-0.
8. **Li, C. H.; Tso, P. L.** 2008. Experimental study on a hybrid-driven servo press using iterative learning control, International Journal of Machine Tools and Manufacture 48: 209-219. https://doi.org/10.1016/j.ijmachtools.2007.08.014.
9. **Wang, Z. R.; Dong, E. B.; Xu, M.; Yang, J.** 2015. Circling turning locomotion of a new multiple closed-chain-legs robot with hybrid-driven mechanism, Advanced Robotics 29(24): 1637-1648. https://doi.org/10.1080/01691864.2015.1071682.
10. **Kireçci, A.; Dulger, L. C.** 2000. A study on a hybrid actuator, Mechanism and Machine Theory 35: 1141-1149. https://doi.org/10.1016/S0094-114X(99)00059-2.
11. **Kütük, M. E.; Halicioglu, R.; Dulger, L. C.** 2015. Kinematics and simulation of a hybrid mechanism: Matlab/SimMechanics, Journal of Physics: Conference Series 574: 012016_1-6. https://doi.org/10.1088/1742-6596/574/1/012016.
12. **Li, H.; Zhang, Y. P.** 2010. Seven-bar mechanical press with hybrid-driven mechanism for deep drawing; Part 1: kinematics analysis and optimum design, Journal of Mechanical Science and Technology, 24(11): 2153-2160. https://doi.org/10.1007/s12206-010-0819-0.
13. **Zi, B.; Sun, H. H.; Zhang D.** 2017. Design, analysis and control of a winding hybrid-driven cable parallel manipulator, Robot Cim-Int Manuf 48 196-208. https://doi.org/10.1016/j.rcim.2017.04.002.
14. **Zi, B.; Cao, J. B.; Zhu, Z. C.; Mitrouchev, P.** 2013. Design, dynamics, and workspace of a hybrid-driven-based cable parallel manipulator, Mathematical Problems in Engineering 914653_1-15. https://doi.org/10.1155/2013/914653.

15. **Zi, B.; Ding, H. F.; Cao, J. B.; Zhu, Z. C.; Kecskeméthy, A.** 2014. Integrated mechanism design and control for completely restrained hybrid-driven based cable parallel manipulators, Journal of Intelligent and Robotic Systems 74: 643-661. https://doi.org/10.1007/s10846-013-9848-0.
16. **Ismail, M.; Lahouar, S.; Romdhane, L.** 2016. Collisionfree and dynamically feasible trajectory of a hybrid cable-serial robot with two passive links, Robot Auton-Syst 80 24-33. https://doi.org/ 10.1016/j.robot.2016.03.001.
17. **Zi, B.; Ding, H. F.; Wu, X.; Kecskeméthy, A.** 2014. Error modeling and sensitivity analysis of a hybrid-driven based cable parallel manipulator, Precision Engineering 38(1) 197-211. https://doi.org/ 10.1016/j.precisioneng.2013.06.002.
18. **Xie, S. R.; Liu, S. M.; Luo, J.; Huang, C; Li, H**. 2015. Trajectory planning of a bionic eye using hybriddriven cable parallel mechanism, Robot 37(4) 395-402. https://doi.org/ 10.13973/j.cnki.robot.2015.0395.
19. **Zhang, Q. S.; Li, R. Q.; Liang, J. J.** 2019.Kinematics and controllability analysis of n-DOF hybrid redundantly driven mechanism, Science Technology and Engineering 19(20) 196-202 (in Chinese).
20. **Zhang, Q. S.; LI, R. Q.; Liang, J. J.** 2022. Kinematics and workspace atlas of 3-PSS/7R hybrid redundantly driven mechanism, Mechanics 28(1): 73-81. http://dx.doi.org/10.5755/j02.mech.28987.

Q. Zhang, R. Li, J. Liang, Y. Wei

KINEMATICS AND TRAJECTORY PLANNING OF 3-PSS/7R SPATIAL HYBRID REDUNDANTLY DRIVEN MECHANISM

S u m m a r y

A novel 3-PSS/7R spatial hybrid redundantly driven mechanism (HRDM) is proposed. The mechanism is driven by constant velocity (CV) motor and servo motor at the same time. The CV motor provides the main power for the system, and the servo motor plays the role of motion regulation. This system not only has the advantages of the traditional mechanical system, such as stable operation, large bearing capacity, but also can output controllable and adjustable flexible trajectory. The degrees of freedom of the mechanism are determined by the middle limb, which is called hybrid redundantly driven limb, which is driven by both CV motor and servo motor. Based on closed vector method, the position equation of the mechanism is established, and the velocity mapping matrix and acceleration change laws of the mechanism are obtained. Further, the necessary and sufficient conditions for the mechanism to realize continuous trajectory and the relationship of rod constraints are obtained. The correctness of the kinematics equation and the smooth and controllable operation of the mechanism are verified by examples. The research results of this paper lay a foundation for the in-depth research and application expansion of spatial hybrid redundantly driven mechanism.

Keywords: 3-PSS/7R parallel mechanism, hybrid redundantly driven mechanism (HRDM), kinematics, trajectory planning.

Received March 6, 2022
Accepted February 15, 2024